Sensors and Actuators A 325 (2021) 112691

Contents lists available at ScienceDirect

Sensors and Actuators A: Physical

journal homepage: www.elsevier.com/locate/sna

Yaw/Heading optimization by drift elimination on MEMS gyroscope

Minh Long Hoang*, Antonio Pietrosanto

Department of Industrial Engineering, University of Salerno, Via Giovanni Paolo II, 132, Fisciano, SA, Italy

ARTICLE INFO

Article history:
Received 24 December 2020
Received in revised form 7 March 2021
Accepted 14 March 2021
Available online 18 March 2021

Keywords:
MEMS
IMU
Accelerometer
Gyroscope
Magnetometer
NMNI
Sensor fusion

ABSTRACT

The main goal of the paper is to achieve a highly accurate measurement of yaw/heading without the support of the Global Positioning System (GPS) and magnetometer by using a practical model based on the principle "No Motion No Integration" (NMNI). The proposed technique removes the drift significantly to optimize the Micro-Electro-Mechanical System (MEMS) gyroscope for the yaw/heading estimation. A "Renovating Model" is added to the NMNI algorithm as a real-time detector for sensor motion state. The 'NMNI' can work effectively with an independent gyroscope or collaborate with other MEMS sensors via fusion algorithms such as Madgwick, Mahony, and Kalman to overcome the limitations of the Global Positioning System (GPS) in the indoor environment. Moreover, the two other critical factors: slope and rotation speed, were examined on sensor behavior to thoroughly verify each filter's pros and cons. The experiments were carried out using a low-cost platform equipped with MEMS as gyroscope, accelerometer, and magnetometer. A Pan Tilt Unit-C46 (PTU-C46) with high accurate positioning was used as a reference angle for both static and dynamic experiments. The results show the considerable advancement of yaw estimation by implementing the NMNI model into the gyroscope thanks to the effective drift removal. Moreover, the fusions between NMNI filter with Mahony and Madgwick accomplish high yaw measurement performance when the sensor on the high slope without magnetometer.

1. Introduction

Nowadays, Inertial Measurement Units (IMUs) has become the critical factor for orientation tracking [1], which are used for multiple applications in the world like robotics, human motion, navigation systems, and many other fields [2–12]. Thus, the requirement of the sensor's quality about highly precise detection for angle orientation like roll, pitch, yaw also increases. Fig. 1 illustrates the Euler angle, generally. Rotation around X-axis, Y-axis, and Z-axis called the roll, pitch, and yaw, respectively. Fundamentally, yaw describes the rotation around the vertical axis, which is crucial in orientation tracking.

This paper works on yaw (heading), which most challenging angle to evaluate. For a static object, roll and pitch can be estimated precisely by accelerometer [13,14], or data fusion with other sensors [15–17]. However, yaw becomes a big challenge for IMU since the accelerometer cannot provide the yaw information when the sensor frame is aligned with the Earth frame. The Z-axis acceleration does not change its reading value when the sensor rotates to the right or left.

The magnetometer's support has been applied popularly to overcome this accelerometer's weakness [18,19]. However, magnetometer requires the high – precision calibration for hard iron as well as soft iron that increases the complexity of the system and also requires the assistance of the GPS [20,21] to guarantee the accuracy of yaw, especially when the strange magnetic distortion appears while the calibration is not updated yet. The scientists already examined the considerable cons of GPS such as Signal Multipath, Receiver and Orbital Clock error. Environmental problems like Ionospheres delay because of the distance and delay in time caused the low accuracy in result [22]. On the other hand, GPS works less effectively in the indoor environment that causes the problem for indoor applications.

The gyroscope can reach the yaw's actual value for a short time, but unfortunately, the 'drift' phenomenon leads to erroneous data. The drift results from the accumulation of the bias offset error and noise in gyroscope measurements utilizing integration through time and yields unacceptable orientation results, highly detrimental to applications that use gyroscopes to determine the orientation [23,24]. Nevertheless, the idea of a gyroscope with minimized drift has been considered as a high potential tool for the yaw estimation. Many scientists have been researching gyroscope [25–27] and drift correction.

The gyroscope drift can be minimized by using gravity-vector compensation [28] or can also be estimated and removed by

* Corresponding author.
E-mail address: mhoang@unisa.it (M.L. Hoang).

https://doi.org/10.1016/j.sna.2021.112691
0924-4247/

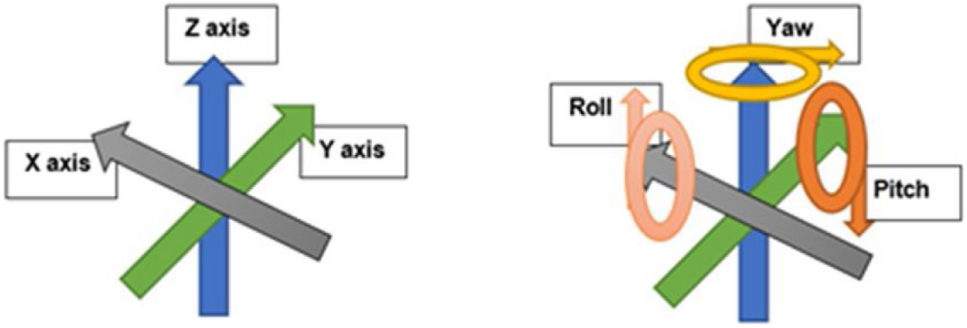

Fig. 1. Euler angles on three axes.

a Wiener-type recurrent neural network [29] for human hand motion. Although the drift is decreased, the gyroscope drift behavior during the angular accumulation may become a complicated case in a dynamic process and should be noticed.

Zero Velocity Update (ZUPT) is a method utilizes the zero velocity condition for stationary case in the indoor navigation, usually applied in Pedestrian Navigation. However, ZUPT can bound the drift effect. However, there are various problems in detection between stationary or dynamic state. Depending on the required level of positioning error growth, the ZUPT execution period is chosen. [30]. By this way, it is less flexible, which can become a disadvantage in automation. A range of detectors detects when the IMU is stationary by using moving acceleration variance [31], magnetometer based [32]. However, the acceleration only varies slightly and less significant when the sensor frame and the Earth frame are the same and only rotate to left or right without inclination. Magnetometer detection can be influenced by iron distortion, caused unexpected errors.

Considering the previous methods, the NMNI technique is presented with the real-time operation to prevent any single portion of drift. This technique was successfully applied to Madgwick filter as described in [51]. In this paper, the NMNI algorithm is directly applied to the gyroscope to accomplish the highest heading estimation efficiency since no additional noise from other sensors can interfere. A threshold is established based on real gyroscope acquisition at a stationary position to realize the sensor state.

From classical mechanics theory, objects will retain the static staete or uniform linear motion until the external force changes this state. Therefore, the stationary state can be reached when the object stops and changes speeds or direction [52]. Thus, sensor state detection is the most essential factor for the whole system successfully processed in the proposed model.

The paper proposes an upgraded NMNI model with a renovating model and in-depth analysis on the yaw in various aspects such as slope or motion speed, which are essential in the practical applications. The NMNI threshold of sensor state detection is calculated based on the real-time acquisition and the update is carried out to adapt to the rise of temperature, which increases the gyro-offset. A model with high precision of update criteria is constructed. The renovating model updates the threshold depending on each gyroscope sensitivity from the datasheet, the current threshold, and the timer value.

For simple analysis, this paper divides the yaw drift into two types: the drift during stationary point as static drift and the drift during sensor motion as dynamic drift. Slope conditions were examined in 2 specific cases for dynamic yaw analysis: static slope and dynamic slope.

- Static slope:yaw angle is stationary, PTU is moved up and down vertically.

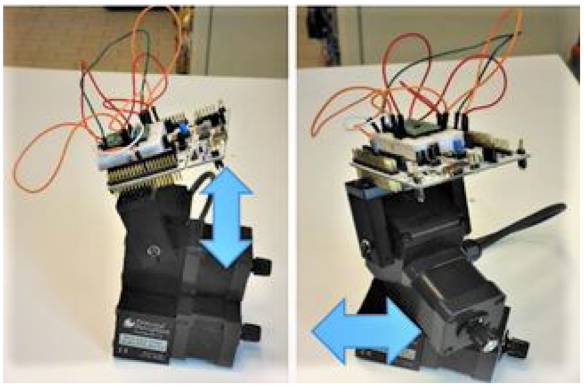

Fig. 2. Static and Dynamic Slope illustration.

- Dynamic slope:yaw angle is in dynamic follow motion of PTU, moved to left and right as Fig. 2 while the sensor is on the slope

The NMNI filter directly works on the gyroscope drift's main problem based on a threshold between stationary state and motion state to prevent the yaw calculation from the additional portion integration.

The principle "No Motion No Integration" and "Renovating Model" construct a real-time operation for the whole system to significantly strengthen the gyroscope characteristic in orientation tracking. The proposed filter combines with Madgwick and Mahony [34] to become filter fusion, such as fused Madgiwck and fused Mahony, to estimate the heading component without magnetometer.

The paper is organized as follows: Initially, a brief description of the most well-known sensor fusion algorithms: Madgwick, Mahony and Kalman [33–36] then the description of the NMNI system about its architecture and its working principle are followed. After this part, the fusion techniques among NMNI filter and other filters were demonstrated as advanced processes. Finally, experimental results and signal analysis will be shown at the end of the paper.

2. Sensor fusion algorithms

2.1. Madgwick filter

The Madgwick filter [34,37] has the good command of combining data from sensors to outcome the advanced signal. This sensor fusion uses the measured acceleration and magnetic field to correct for gyroscopic drift [38]. Thus, this paper only briefly demonstrates the algorithms' idea with the fusion of accelerometer and gyroscope.

In the Madgwick filter, gyroscope noise is minimized by acceleration and magnetic data, based on gradient descent in every update step based on the quaternion [39–41].

The angular rate ωx, ωy, ωz are acquired from the x, y, z axes of the sensor frame which are represented in S_ω vector (in rads^{-1})

$$S_\omega = [\,0\ \omega_x\ \omega_y\ \omega_z\,] \tag{1}$$

${}^S_E\hat{q}$ describes the orientation of the Earth frame relative to the Sensor frame in the term of the quaternion.

$${}^S_E\hat{q} = [q_0\, q_1\, q_2\, q_3\,] \tag{2}$$

The quaternion derivative describes the rate of change of orientation of the earth frame relative to the sensor frame ${}^S_E\dot{q}$ can be calculated [3] as equation

$${}^S_E\dot{q} = \frac{1}{2} {}^*{}^S_E\hat{q} \otimes S_\omega \tag{3}$$

The orientation of the earth frame relative to the sensor frame, the angular rate at time t called as ${}^S_E q_{\omega,t}$, $S_{\omega,t}$ respectively at sampling period Δt.

With ${}^S_E\hat{q}_{t-1}$ being the previous estimate of orientation:

$${}^S_E\dot{q}_{\omega,t} = \frac{1}{2} {}^S_E\hat{q}_{t-1} \otimes S_{\omega,t} \tag{4}$$

$${}^S_E q_{\omega,t} = {}^S_E\hat{q}_{t-1} + {}^S_E\dot{q}_{\omega,t}\Delta t \tag{5}$$

With the accelerometer value a_x, a_y, a_z, the Madgwick for yaw estimation includes four main steps:

Step 1:Rate of change calculation

$$\Delta q = \frac{1}{2} q \otimes \omega = \frac{1}{2} \begin{pmatrix} -q_1\omega_x - q_2\omega_x - q_3\omega_z \\ q_0\omega_x + q_2\omega_z - q_3\omega_y \\ q_0\omega_y - q_1\omega_z + q_3\omega_x \\ q_0\omega_z + q_1\omega_y - q_2\omega_x \end{pmatrix} \tag{6}$$

Step 2:Corrective step computation δs based on gradient descent algorithm

$$\begin{pmatrix} 4q_0q_2^2 + 2q_2a_x + 4q_0q_1^2 - 2q_1a_y \\ 4q_1q_3^2 - 2q_3a_x + 4q_0^2q_1 - 2q_0a_y - 4q_1 + +8q_1^3 + 8q_1q_2^2 + 4q_1a_z \\ 4q_0^2q_2 + 2q_0a_x + 4q_2q_3^2 - 2q_3a_y - 4q_2 + 8q_2q_1^2 + 8q_2^3 + 4q_2a_z \\ 4q_1^2q_3 - 2q_1a_x + 4q_2^2q_3 - 2q_2a_y \end{pmatrix} \tag{7}$$

Step 3:The quaternion change rate δq can be corrected with δs, calculated in (7), and integrated as follows.

$$\Delta q' = \Delta q - \beta\delta s \tag{8}$$

$$\dot{q} = \Delta q' \tag{9}$$

$$q_t = q_{t-1} + \Delta q'\Delta t \tag{10}$$

Step 4:Yaw calculation

$$\text{yaw} = tan^{-1}\left(\frac{q_1q_2 + q_0q_3}{0.5 - q_2^2 - q_3^2}\right) \tag{11}$$

Where β is the divergence rate.

With the absence of magnetometer, the Madgwick yaw suffers a large drift from the gyroscope because the accelerometer can not detect the vertical axis's body change. Hence, the combination with NMNI filter is the promising approach that will be represented in detail in section IV.

2.2. Mahony filter

The Mahony filter corrects the rotation vector S_ω, based on a Proportional Integral (PI) controller on the correction vector. The error vector is defined as below:

$$e = a \times d \tag{12}$$

Where a is the accelerometer vector, d is the gravity vector's direction as given by the estimated attitude.

Generally, the Mahony algorithm is expressed as following steps where Ki and Kp are the integral and proportional adjustable gains.

Step 1:Estimation of gravity vector d from quaternion

$$d = 2\begin{pmatrix} q_1q_3 - q_0q_2 \\ q_0q_1 + q_2q_3 \\ q_0^2 + q_3^2 - \frac{1}{2} \end{pmatrix} \tag{13}$$

Step 2:Calculation of error vector

$$e = a \times d$$

Step 3:Vector integration calculation

$$I_n = I_{n-1} + eKi\,\Delta t \tag{14}$$

Step 4:Proportional vector

$$\omega' = \omega + K_p + I_n \tag{15}$$

Step 5: Rate integration of change using $\dot{q} = \frac{1}{2} q \otimes \omega$'

$$\begin{aligned} q_n &= q_{n-1} + \frac{1}{2} q_{n-1} \otimes \omega'\,\Delta t \\ &= q_{n-1} + \frac{1}{2} \begin{pmatrix} -q_1\omega_x' - q_2\omega_x' - q_3\omega_z' \\ q_0\omega_x' + q_2\omega_z' - q_3\omega_y' \\ q_0\omega_y' - q_1\omega_z' + q_3\omega_x' \\ q_0\omega_z' + q_1\omega_y' - q_2\omega_x' \end{pmatrix} \end{aligned} \tag{16}$$

Step 6:Yaw calculation

$$\text{yaw} = tan^{-1}\left(\frac{q_1q_2 + q_0q_3}{0.5 - q_2^2 - q_3^2}\right) \tag{17}$$

2.3. Kalman filter

Kalman filter is a useful tool to remove the random noise by using the prediction and update [42]. In this case, the angular velocity fuses with a magnetometer to reduce the magnetic heading's unexpected variation.

Kalman model:

$$x_{t+1} = F.x_t + B_t.u_t + w_t \tag{18}$$

$$z_{t+1} = H.x_{t+1} + v_{t+1} \tag{19}$$

Where x_t, x_{t+1} are the system's state vectors at time t and t + 1, u_t is the input vector at time t, z_{t+1} is an observation (or measurement) at time t + 1

- F is the state transition model that relates the current states to the next states
- B_t is the control input model which is applied to the control vector u_t;
- H is the observation model that maps the true state space into the observed space
- w_t is the state transition noise is attained by a zero-mean normal distribution with the process noise covariance matrix Q[k] with $w_t \approx N(0, Q)$.

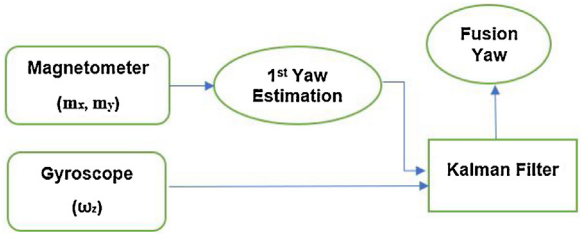

Fig. 3. Kalman filter for heading estimation.

$$Q[k] = \begin{bmatrix} Qacc & -\Delta T \\ 0 & Q\,bias \end{bmatrix} \tag{20}$$

This matrix includes the estimated state from the accelerometer variance Qacc and the variance of bias Qbias multiplied by the time interval ΔT.

- Like w_t, with R is the variance of the measurements, v_t is the noise measurement $v_t \approx N(0, R)$.

The heading estimation from magnetometer:

$$\psi = tan^{-1}\left(\frac{m_x}{m_y}\right) \tag{21}$$

Where m_x, m_y are magnetic field measured surround axis x, axis y respectively.

Eq. 21 yields local magnetic heading, which may happen to be the opposite of proper heading, and often deviates by as much as 20–30° from the latter one. To minimize the noise, the yaw estimation from the magnetometer fuses with ω_z from the gyroscope. Here, ω_z with ΔT can detect the proper value of yaw for a short time, which is a good tool to minimize the short-term distortion on heading estimation. As a result, the Kalman filter generates accomplishes the fusion yaw, as demonstrated in Fig. 3.

3. The NMNI algorithm

Firstly, n samples are collected from the angular velocity bias Z_i and then averaged as the turn-on zero-rate level Z_{bias} to be removed from the next data $Z_{gy}[k]$.

$$Z_{bias} = \sum_{i=0}^{n} Z_i \tag{22}$$

$$Z_{gy}[k] = Z_{gy}[k] - Z_{bias} \tag{23}$$

This step is essential for the integration progress to reach the actual value from the sensor.

3.1. "No Motion No Integration" principle

Usually, the gyroscope calculates the yaw by integrating the angular rate from the z-axis, called Zgy. However, the drift misleads the obtained result especially when the sensor stays at rest. [9]. The NMNI has the mission to eliminate every single portion which contributes to this drift problem

In the start-up phase, the sensor is in a no-motion state. The abs value of Zgy is stored with the index of the sample as i (i is an integer number corresponding to the window size, i = 1), then the filter will keep a Zgy with the highest value as 1st threshold.

$$Z_{th} = \max\{|Z_{gy}[1]|, |Z_{gy}[2], \ldots |Z_{gy}|[i]\} \tag{24}$$

Where Z_{th} is the first threshold as the boundary between stationary and dynamic conditions.

A filter is used to select the maximum data as Z_{th} becoming the boundary between static and dynamic circumstance. The principle works on the comparison between real-time measured $Z_{gy}[k]$ and threshold value Z_{th}.

- $Z_{gy}[k] > Z_{th} \longrightarrow$ sensor is in the dynamic case.
- $Z_{gy}[k] \leq Z_{th} \longrightarrow$ sensor is in the static case.

Here, the gyroscope characteristic can be varied due to the temperature change [43], so the Z_{th} should be updated in real-time as described in the next section.

3.2. Frame for "Renovating model for $\Delta Z_{th.}$"

This model aims to update the threshold Z_{th} guarantee the system's stability because the offset can be varied due to the noise or long-time operation. In this part, two stages are described in detail to demonstrate the update process of the NMNI system, including 2 stages:

Stage1 generates the checking period by using based on the time loop and the time from the stopped moment to that cycle end. This checking procedure is the practical way to decide whether the NMNI system should renovate the value of Z_{th}.

Stage 2 creates the condition for threshold update.

The renovating model for ΔZ_{th} is processed under a virtual frame, as shown in Fig. 5.

Stage 1. Timer (the 1 st condition)

Firstly, the programming system is implemented in the real-time clock following the structure below

•While ()

T_start // (starting time of a loop)

T_end // (ending time of a loop)

Here, each time the sensor stays at rest, a new time clock is set called T_rest, indicating the moment sensor just pauses its motion. The user may select one or more cycles (optional) depending on the time loop and application type.

$$\text{Time loop} = \Delta t1 = \text{T\_end} - \text{T\_start} \tag{25}$$

The checking time on behalf of the number of cycles in which the user wants to check whether |Zgy| > Z threshold during the immobile period. In this case, this condition is satisfied, that Zgy will be the new $Z_{threshold}$. Otherwise, the $Z_{threshold}$ has remained as of old value that shows that the gyroscope still works at the same circumstance as before

At 1 st state, the time remaining from T_rest to T end:

$$\Delta t2 = \text{T\_end} - \text{T\_rest} \tag{26}$$

Time_check is counted as the amount of time after the sensor stops as 2nd state in Table 1.

$$\text{Time\_check} = c * \Delta t1 + \Delta t2 \tag{27}$$

Where c is the number of cycles, the user would like to check. The user should compromise between Time_check and the paused time of application. In this case, c = 1 so the checking period of threshold will be the sum of the time execution from stop moment to the loop end and a next time loop.

The executive order of the time clock is established following the below regulation (Table 2).

Stage 2. Updating threshold (UT-the 2nd condition)

In the 2nd condition, to avoid updating the Z_{th} in the sensor's slow motion, an UT was considered to assure the whole operating system's accuracy.

The 2nd condition to update the Z_{th} is implemented as:

$$\left|Z_{gy}\right| - Z_{th} < UT \tag{28}$$

At this step, if the user sets UT too small $\longrightarrow$ the Z_{th} slowly updated and even ignored many cases satisfied the 1 st condition.

Table 1
Kalman operating principle.

Prediction	Update
Estimation State (a priori): $x_{t+1} = F\ x_t + B_t\ u_t$	Innovation : $y_{t+1} = z_{t+1} - H\ x_{t+1}$
Error covariance: $P = F\ P\ F^T + Q$	Innovation covariance : $S = H\ P\ H^T + R$
	Optimal Kalman gain: $K = P\ H^T\ S^{-1}$
	State estimate (a posteriori): $x_{t+1} = x_{t+1} + K\ y_{t+1}$
	Estimate covariance: $P = (I - K\ H)\ P$

Table 2
The order of time execution before and after setting timer.

Index	1st state (T_rest just triggered)
1	T_start
2	T_rest
3	T_ end

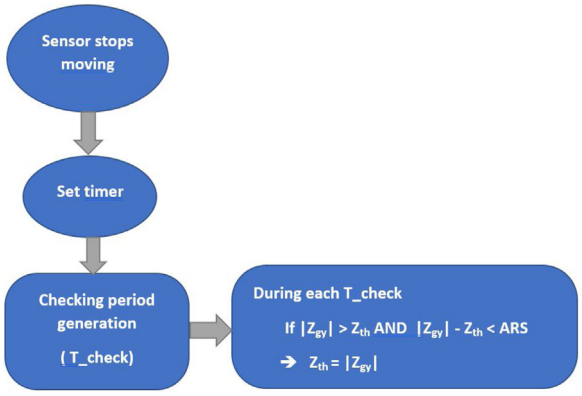

Fig. 4. NMNI update model.

If the user sets UT too high $\longrightarrow Z_{th}$ update also in the dynamic period or inappropriate value due to spike and the value is incorrect.

Hence, the UT should be equivalent to Angular rate sensitivity (ARS), which is up to each gyroscope's datasheet. The slowest motion leads to the least significant bit (LSB) variation and 1 LSB ≈ ARS.

3.3. Overview of the NMNI model

"Renovating Model for Z threshold" is processed to help the system prevent the "drift" most effectively and achieve the proper estimation for yaw. The system was illustrated in Fig. 4.

During the static state, each checking period:

$$\text{If} |Z_{gy}| > Z_{th} \text{AND} |Z_{gy}| - Z_{th} < \text{ARS} \longrightarrow \text{new} Z_{th} = |Z_{gy}|$$

With the implementation of the "NMNI" algorithm, the heading measurement will be improved apparently. The loop can be repeated every time the sensor stays at rest to check the update for the threshold value until the sensor's next motion. Fig. 5 shows the whole system of the NMNI algorithm.

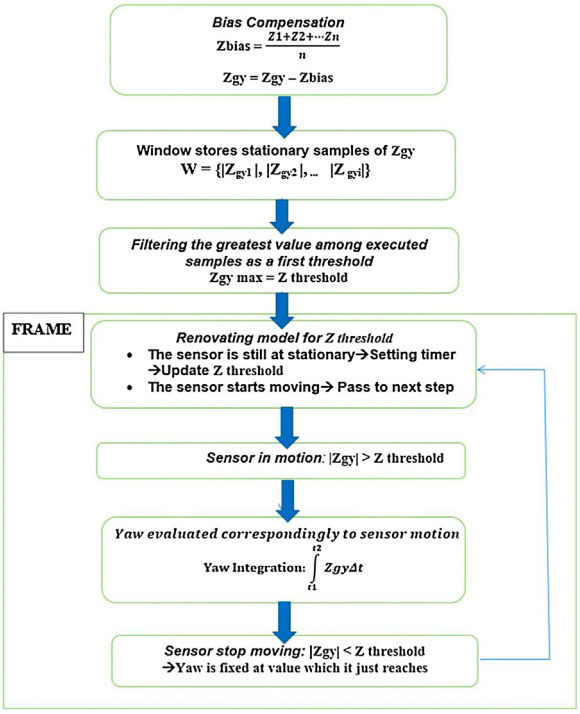

Fig. 5. Overview of NMNI system.

4. Filter fusion Madgwick/Mahony and NMNI

When the sensor stays on a slope, the sensor frame is different from the Earth frame, so the Gyroscope yaw does not rely on the rate integration of the z-axis only but also the other two axes. Meanwhile, Madgwick and Mahony filter is able to calculate the orientation of the sensor frame relative to the earth frame by the quaternion and the gradient descent algorithm.

Furthermore, the quaternion has a good command of rotating a vector from the body frame to the Earth frame that is practically useful for the slope's IMU sensor operation. Fig. 6 shows the fusion process between Madgwick/Mahony filter with NMNI algorithm.

Basically, before entering the Madgwick or Mahony filter, the gyroscope data pass through the NMNI filter firstly.

- $Z_{gy} > Z_{threshold} \rightarrow$ sensor is in motion: $\omega_x, \omega_y, \omega_z$ enter the Madgwick filter normally.
- $Z_{gy} \leq Z_{threshold} \rightarrow$ sensor is stationary: $\omega_x, \omega_y, \omega_z$ have zero value.

This fusion technique overcomes the dynamic integration problem on the NMNI filter's slope and the random drift of the Madgwick filter without magnetometer.

5. 'Improved NMNI' model

At this point, the NMNI filter has superiority in yaw evaluation because the noise of the accelerometer and magnetometer does not influence it. Meanwhile, the hybrid between Madgwick and NMNI is the optimized solution when the sensor on the slope.

Thus, a completed version of NMNI was integrated, relied on the best features from both algorithms, and divided into 2 modes as shown in Fig. 7:

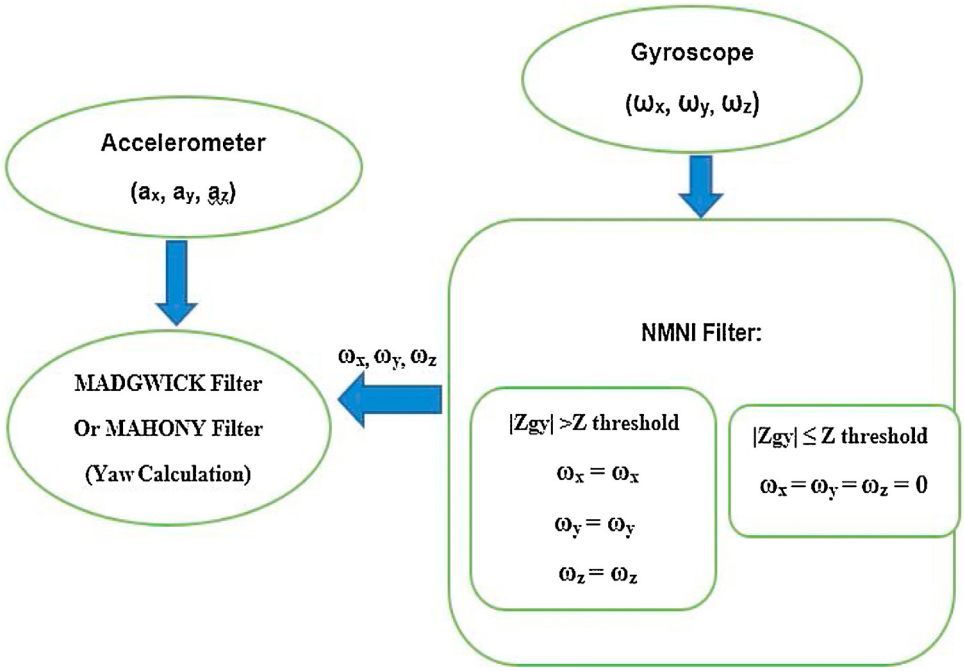

Fig. 6. The fusion between Madgwick /Mahony and NMNI block chain.

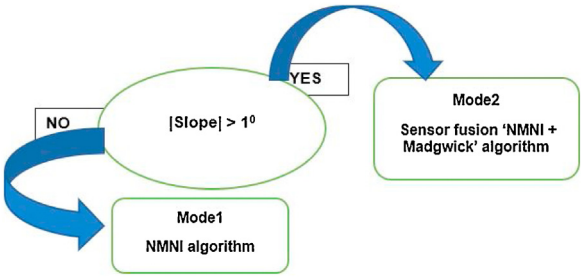

Fig. 7. The improved NMNI block sequence.

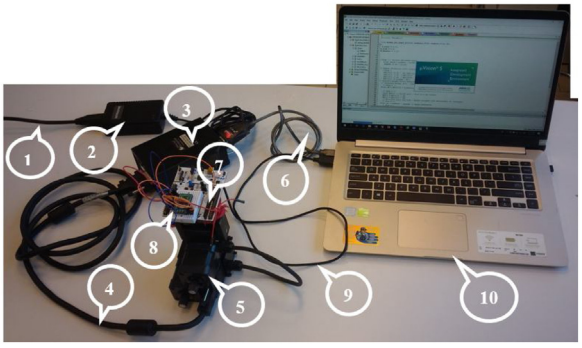

Fig. 8. Test bench for experiment.
1. Power Supply cable for PTU-C
2. AC/DC Power Supply
3. PTU-C Controller
4. 7ft Cable
5. PTU-C46 Pan Tilt Unit
6. RS232 cable
7. NUCLEO-F401RE Board
8. LSM9DS1 Sensor
9. USB Mini Cable
10. Computer with Keil uVision & STM32CubeMX program

- Mode1: Sensor frame is the same as the Earth frame. The NMNI filter independently works at this circumstance to achieve the highest efficiency of yaw estimation.
- Mode2: Sensor frame and the Earth frame are different due to the slope case. At this time, the 'Improved NMNI works as the sensor fusion 'Madgwick and NMNI'.

6. Experimental setup

The experimental sensors are the LSM9DS1 from STMicroelectronics [44,49], which is made up of accelerometer, gyroscope and magnetometer. Here, the accelerometer works in range of ±4 g, the gyroscope range is ± 245°/s, full magnetic scale is ±8 G. The bias of gyroscopes is ± 0.015°/s and accelerometer bias is about 11.25 mg.

The algorithms has been implemented into an ARM Cortex-M4 based microcontroller STM32F401RE by STMicroelectronics [45,46], with NUCLEO-F401RE [47,48]. The sensor is connected to the MCU development via an Inter-Integrated Circuit (I2C) communication line.

The oriental device is the Pan-Tilt Unit Controller (PTU-C46) [50], which has a resolution 0.051° per position with accurate positioning of cameras. The LSM9DS1 is assembled on PTU-C for tracking Euler angles like Fig. 8.

The concerned model has a critical role in a wide range of applications such as robotics process automation or navigation. For example, the robot arm needs to rotate to the right for 30° for picking an object. This procedure requires high precision of yaw measurement to guarantee the robot arm moves at correct angle. In navigation, side-to side movement of the vehicle is important to detect for the ship or car, etc. since the GPS signal can be lost or poor due to external interference from obstacle and region.

7. Experimental analysis

To achieve a stable transferring signal between the sensor and the computer, the Output Data Rate (ODR) of accelerometer and gyroscope was set at 119 Hz, equivalent to 0.008 s of time period. Besides, the magnetometer ODR is 80 Hz, about 0.0125 s of period. Hence the system acquisition carried out at 119 Hz for the filter without magnetometer and at 80 Hz vice versa.

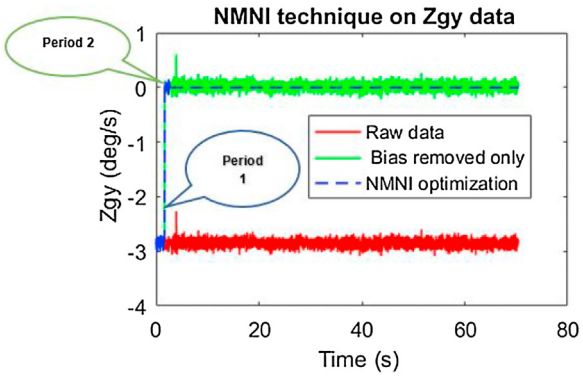

Fig. 9. NMNI technique on Zgy.

Table 3
Zgy variation at static case.

Z-GY NOISE VARIATION ABOUT A MINUTE			
Variation (^{0}/s)	Raw data	No bias	After NMNI
Mean	2.854	0.058	0
Standard deviation	0.071	0.044	0

After many simulations with adjustable parameters, the best value of each algorithm factor for the experiment was chosen to operate at their high effective performance as follow:

- Madgwick:β = 0.42.
- Mahony:Kp = 0.6; Ki = 0.01
- Kalman:Qacc = 0.01; Qbias = 0.03; R= 0.01.

7.1. 'NMNI' algorithm on gyroscope behavior

In the 1st part of the experiment, the angular rate of Zgy is characterized to demonstrate the working process from initial bias removed to NMNI technique. The red line shows the raw data of Zgy; the green line shows the signal after bias extraction, and the NMNI optimization displays on the blue line with the marker as Fig. 9.

- Period 1: 190 raw samples are collected to remove the bias of the gyroscope.
- Period 2: the 1st threshold value is filtered from the next 119 samples.

After the first 1.6 s, the initial bias is removed then the 1st threshold is filtered after 1 s to generate zero-noise signal continuously at the stationary position. It is easy to observe that despite initial bias elimination, the Zgy still varies considerably Table 3 reports the noise variation in absolute value. NMNI technique works perfectly in the role of noise elimination.

The NMNI filter function was examined on the yaw measurement, calculated by gyroscope at the static point. As shown in Fig. 10, the drift pulls down the yaw value dramatically, about 1° per second. However, after applying the NMNI filter, the yaw was maintained around 0° without any strange spike. Here, the test was directly observed from the state where 1st threshold was already collected.

For 60 s, the table value is obtained from the large number of data (≈ 7140 samples). Here, numerous samples were calculated for behavior observation of long-term drift.

Table 4 indicates the huge advanced feature after applying the NMNI filter.

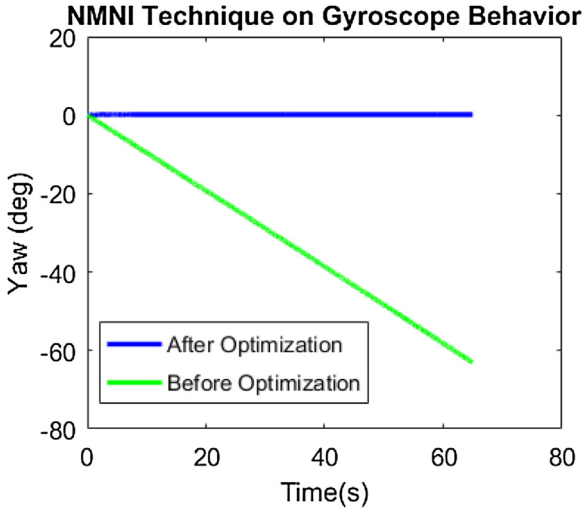

Fig. 10. Static drift of Gyroscope Yaw before and after optimization.

Table 4
Analyzed data from Gyroscope drift.

GYROSCOPE DRIFT BEFORE AND AFTER NMNI ALGORITHM UNDER STATIC CONDITION		
Yaw drift (°)	Before	After
min	0.015	0
max	63.075	0
mean	31.403	0
Standard deviation	18.199	0

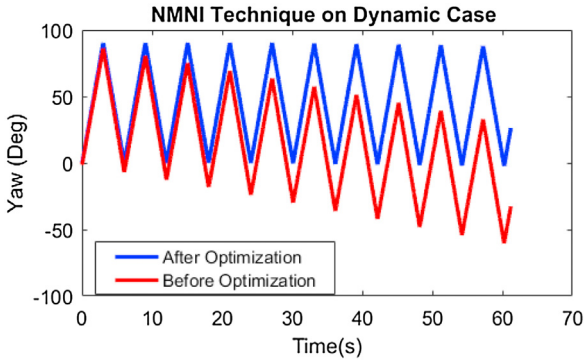

Fig. 11. NMNI filter on Yaw measurement from gyroscope.

For the dynamic drift test, the device PTU-C was controlled from 0° to 90° back and forth for a minute. Each time the PTU-C reaches the edged points: 0° or 90°, this device is in stillness in a concise period of time due to inertia, which is the resistance of a physical object to change in its direction of motion. With this motion inertia, it is easy to observe the cumulative drift of gyroscope characteristics without an optimized solution.

It drifts down about 50 degrees because the integration accumulates the noise over time and turns noise into the drift, which yields incorrect results. The yaw is only maintained in the right range after the NMNI filter removes the noise. Fig. 11 shows the improvement of gyroscope drift before and after using the NMNI filter

To verify the stability and accuracy of the NMNI algorithm, the sensor was tested by rising and declining processes with differential step 30° in the range (0°, 90°). Each indicated angle remained continuously for 1200 samples to observe the gyroscope drift.

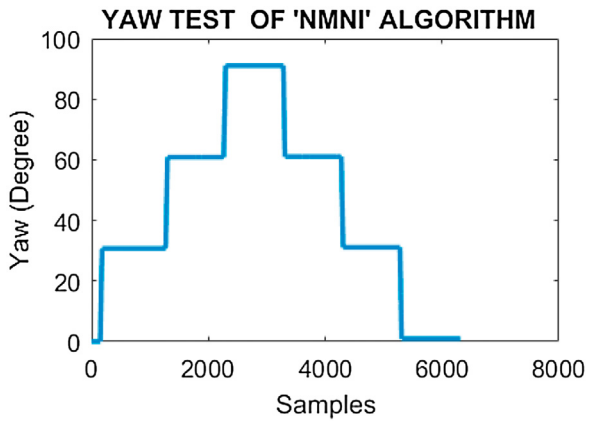

Fig. 12. Yaw behavior for testing stability after NMNI filter.

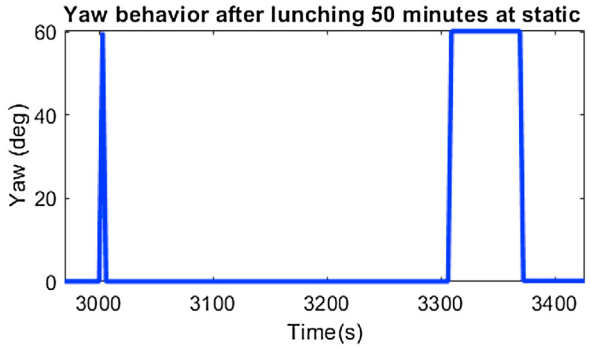

Fig. 13. Yaw behavior after long time operation.

Table 5
Madgwick static drift analysis.

Yaw drift (°)	Before Fusion	After Fusion
min	5.871	0.010
max	179.96	0.064
mean	39.766	0.041
Standard deviation	111.559	0.007

The sensor perfectly attains the appropriate angle at the rising process, and almost no drift occurs during the stationary interval. When the sensor is moved down from 90° to each 0°, the angles only slightly vary respectively to the rising process as shown in Fig. 12. The system successfully realizes the static state to prevent the drift at this state successfully and detects the dynamic state to follow the physical sensor motion properly.

Another test was carried out to observe the yaw behaviour after long time of operation. In this test, the sensor stays at the static point of 0° for 50 min, then starting the rotation from 0° to 60° then returns to 0°. After staying at the rest for 5 min, another rotation is carried out from 0° to 60°, then resting for a minute before spinning back to 0°. The speed of PTU-C rotation is about 20°/s. As shown in Fig. 13, the yaw has good command of tracking the device rotation in term of long-time operation.

7.2. NMNI on sensor fusion

The 2nd part tests on the Madgwick without magnetometer. And as shown in Fig. 14, the yaw drift of Madgwick is speedy, and when it reaches the −180°, it flips to 180° just for less than a minute. Consequently, the Madgwick filter cannot be used for yaw estimation without magnetometer [25]. The NMNI corrects the signal behavior and keeps it at the proper value as reported in. Table 5.

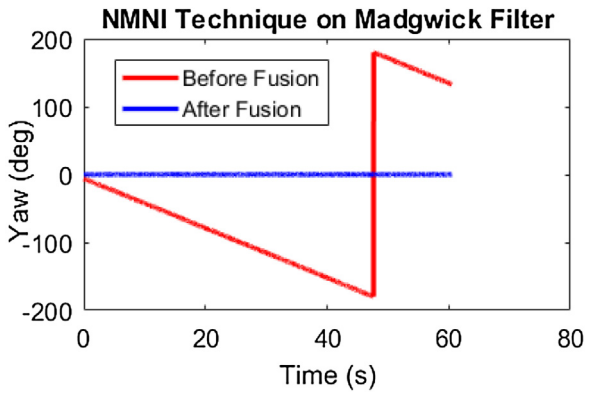

Fig. 14. Madgwick static drift (no magnetometer) before and after fusion.

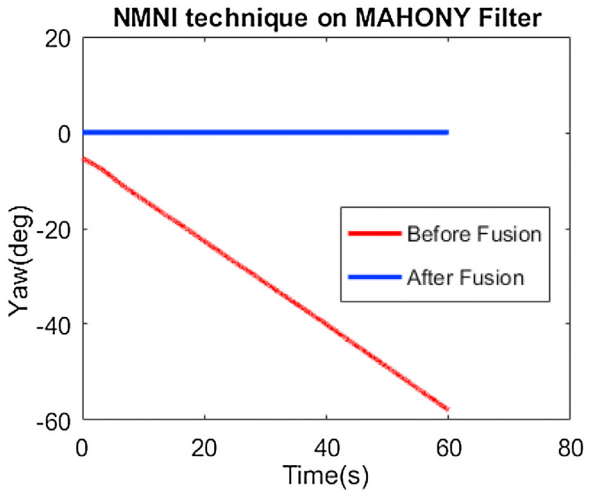

Fig. 15. Mahony static drift (no magnetometer) before and after fusion.

Table 6
Mahony static drift analysis.

Yaw drift (°)	Before Fusion	After Fusion
min	5.342	0.282
max	57.924	0.413
mean	31.407	0.372
Standard deviation	15.217	0.043

Similarly, the Mahony yaw suffers the large drift as shown in Fig. 15, approximately 1° /s, and it only behaves in the right way after fusing with the NMNI method. There is only small variation on the fused Madgwick and fused Mahony due to the acceleration components (Table 6).

7.3. Comparison of the positioning algorithms

The precise experiments were built in both dynamic and static circumstances for Madgwick with the magnetometer, Kalman, and NMNI filter to observe a new algorithm's pros and cons. The hybrid of Madgwick and NMNI filter is also recorded on the table result, and its graph will be demonstrated separately in the next part for a clear illustration.

For the dynamic test, the PTU-C rotates 11 turns continuously at three velocity levels 30°/s, 40°/s, and 60°/s, as demonstrated in Fig. 16. The data evaluation is calculated by the Root Mean Square Error (RMSE).

Table 7
Error calculation under dynamic condition.

ESTIMATION ERRORS UNDER DYNAMIC CONDITIONS					
PTU-C Speed (°/s)	Madgwick with magnetometer RMSE (°)	Kalman RMSE (°)	NMNI RMSE (°)	Mahony + NMNI RMSE (°)	Madgwick + NMNI RMSE (°)
30	0.75	0.68	0.34	0.67	0.70
40	0.77	0.95	0.34	0.84	0.72
60	0.86	1.37	0.48	0.95	0.78

Table 8
Error calculation under static condition.

ESTIMATION ERRORS UNDER STATIC CONDITIONS					
PTU-C angle	Madgwick with magnetometer RMSE (°)	Kalman RMSE (°)	NMNI RMSE (°)	Mahony + NMNI RMSE (°)	Madgwick + NMNI RMSE (°)
0	0.65	1.29	0.01	0.08	0.03
30	0.73	0.59	0.35	0.40	0.41
60	0.61	1.33	0.72	0.86	0.67
90	1.55	0.95	0.77	1.51	1.09

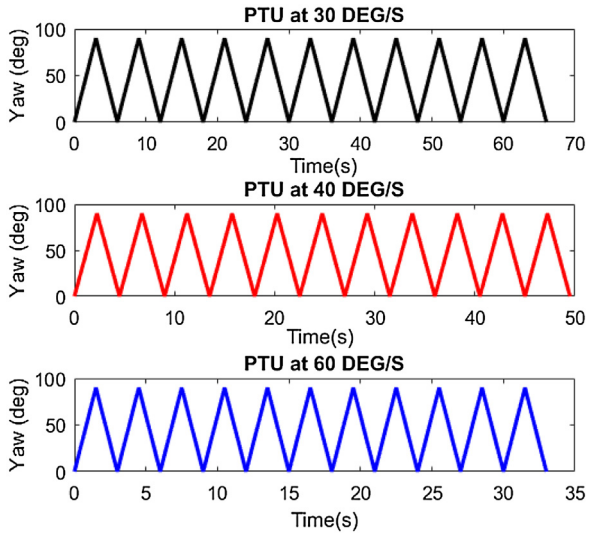

Fig. 16. Test reference for dynamic case at various speeds.

As recorded in Table 7, the higher speed of motion conducts more considerable RMSE because it is more difficult for the MEMS sensor's internal cells to catch up and react to high velocity.

The Kalman filter has considerable RMSE at high speed of motion. When the rotation reaches high speed, complex mathematic requires a longer time of operation. The NMNI and Madgwick filter show impressive achievements. Their fusion accomplishes a smaller value of Madgwick RMSE but higher than the NMNI ones in dynamic and static analysis.

For the static test, PTU-C was controlled to indicate from 0° to 90° with a differential step at 30°, 100 samples were extracted from each angle to calculate the RMSE like Table 8. Larger angle, bigger RMSE, the NMNI, and fused Madgwick have better accuracy than others, while Madgwick with magnetometer estimation is quite balanced from until 60°. The Kalman has the most significant error at the starting point, but it is better at a successive angle.

7.4. Slope case

For the inspection of the slope case which is the most sensitive situation for IMU sensors. The analysis focuses on:

- The static slope: the yaw was kept at a constant angle, but the pitch was varied from 0° to 45°.

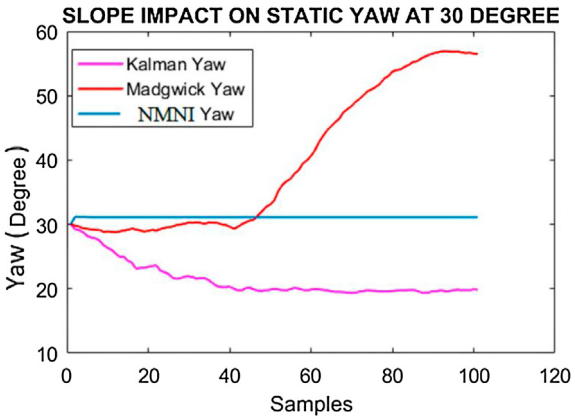

Fig. 17. Influence of slope on static yaw.

- The dynamic slope: the pitch was always kept at 45° (highest possible tilt of PTU-C configuration), then, the device continuously from 0° to 90° and vice-versa about 11 turns.

7.4.1. Static slope (PTU only inclines, no yaw rotation)

Fig. 17 and Table 9 demonstrate how slope influences each algorithm differently. In the case of Madgwick with magnetometer and fused Mahony filter, the higher value of the angle is more susceptible to the slope alteration. In contrast, the slope shows less impact on the Kalman filter when yaw increases.

Both NMNI and its fusion with Madgwick are immune to the static slope. The yaw measured by the gyroscope mainly depends on the z-axis and when the slope rises or lows down, only making the change of data from the X-axis or Y-axis.

Logically, the Madgwick yaw varied due to static slope according to its mathematic equation in the corrective step. However, after fusing with NMNI, all the gyroscope angle rates have no value when the Z-axis has no motion. Thank to this feature, the fusion filter has a minimal change in this case. The vibration of PTU-C only causes little fluctuation during its operation.

7.4.2. Dynamic slope (PTU inclines and rotates the heading)

The more formidable challenge is set up for NMNI and its filter fusion. The PTU tilts $45^{0,}$ then turns back and forth from 0° to 90° at the velocity of 60°/s, as shown in Fig. 18. The acquired results have a small delay with respect to reference because of Serial Port Transmit Data and Receive Data.

The advantage of filter fusion over independent NMNI is examined in the dynamic slope. This test was only carried out with the

Table 9
Error calculation under static slope condition.

ESTIMATION ERRORS ON STATIC SLOPE					
PTU-C angle (°)	Madgwick with magnetometer RMSE variation (°)	Kalman RMSE variation (°)	NMNI RMSE variation (°)	Mahony + NMNI RMSE (°)	Madgwick + NMNI RMSE variation (°)
0	1.34	37.99	0.01	1.09	0.03
30	11.69	24.14	0.01	1.67	0.03
60	22.05	11.47	0.01	1.94	0.03
90	30.88	2.38	0.01	2.01	0.03

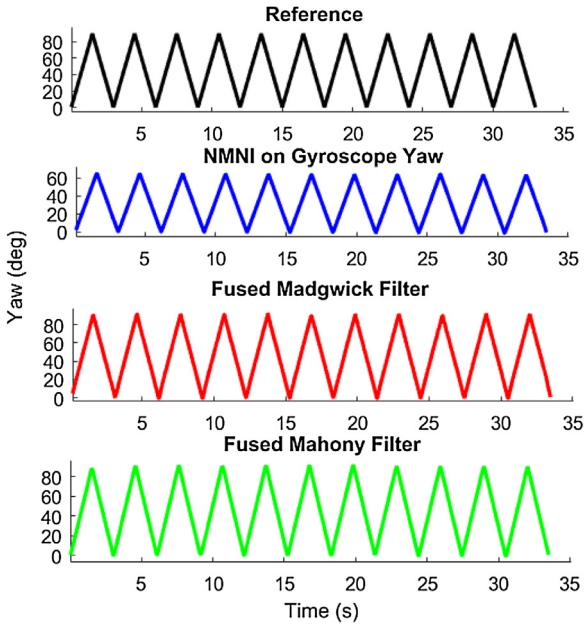

Fig. 18. Comparison between 3 fused filters on dynamic slope.

Table 10
Error comparison between 2 fused filters under dynamic slope condition.

DYNAMIC ESTIMATION ERRORS ON SLOPE		
PTU-C Speed (°/s)	Mahony + NMNI RMSE (°)	Madgwick + NMNI RMSE (°)
30	0.81	0.69
40	0.83	0.82
60	0.87	0.87

3 algorithms that are less vulnerable to the static slope than the previous table. The yaw result from the NMNI gyroscope only can reach approximately 65° while the PTU-C spins to 90° dues to the missing integration portion when the sensor frame differs from the Earth frame.

Nevertheless, with the support of the Madgwick and Mahony filter, the NMNI yaw is obtained at the proper angles thanks to its self-contained ability for deriving global orientation that is extremely helpful for monitoring body kinematics. Table 10 indicates the superior performance of fused

Madgwick over fused Mahony under the slope condition.

8. 'Improved NMNI' performance

As reported in Tables 11 and 12, the completed algorithm with the name 'Improved NMNI' comprises two pros from independent NMNI and 'Fused Madgwick'. In the case the sensor frame is the same as the Earth frame, the 'Improved NMNI' works as independent 'NMNI'; otherwise, this algorithm follows the operation of 'Fused Madgwick.'

Table 11
Overall data of 'Improved NMNI' filter in the static case.

IMPROVED NMNI UNDER STATIC CONDITIONS	
PTU-C angle (°)	Madgwick + NMNI RMSE (°)
0	0.01
30	0.35
60	0.72
90	0.77

Table 12
Overall data of 'Improved NMNI' filter in dynamic case.

IMPROVED NMNI UNDER DYNAMIC CONDITIONS		
PTU-C Speed (°/s)	DYNAMIC RMSE (°)	DYNAMIC ON SLOPE RMSE (°)
30	0.34	0.79
40	0.34	0.82
60	0.48	0.90

9. Conclusion

The paper described a new algorithm to explore the gyroscope's full potential in the role of orientation tracking. The NMNI filter, as well as other powerful filters, were implemented into the IMU sensor appropriately under the verification of accurate positioning device PTU-C46. As a result, the NMNI filter can collaborate with other types of filters like Madgwick to strengthen its performance in the global orientation that brings fresh filter fusion ideas.

The experimental results indicate that NMNI achieves a high efficiency of yaw estimation with small ERMS, maximum of about 0.77° at 90° for static and 0.48° at the dynamic case. The magnetometer function was successfully implemented into Kalman and Madgwick for yaw measurement that operates well when the sensor frame and Earth frame are aligned.

For the slope case, the combination of the NMNI technique with Madgwick and Mahony filters accomplish high accuracy in heading estimation and overcome the concern of iron distortion, thanks to the absence of magnetometer. This filter opens a new approach for the gyroscope evolution, opening a new way about Euler angle estimations with the only gyroscope. The proposed method opens a new approach to heading measurement and potentially becomes a promising key in orientation with less complicated but effective processes.

Authorship contributions

Category 1

Conception and design of study: Heading Estimation, NMNI filter

acquisition of data: gyroscope, yaw value from sensor fusion and NMNI filter

analysis and/or interpretation of data: heading acquisition comparison between all the concerned algorithms.

Category 2

Drafting the manuscript: Heading Optimization by Drift Elimination on MEMS Gyroscope,

revising the manuscript critically for important intellectual content: Yaw/Heading Optimization by Drift Elimination on MEMS Gyroscope

Category 3

Approval of the version of the manuscript to be published.

M.L. Hoang

A. Pietrosanto

Declaration of Competing Interest

All authors have participated in (a) conception and design, or analysis and interpretation of the data; (b) drafting the article or revising it critically for important intellectual content; and (c) approval of the final version.

This manuscript has not been submitted to, nor is under review at, another journal or other publishing venue.

The following authors have affiliations with organizations with direct or indirect financial interest in the subject matter discussed in the manuscript: *Yaw/Heading Optimization by Drift Elimination on MEMS Gyroscope*

References

[1] M. Carratù, S. Dello Iacono, M.L. Hoang, A. Pietrosanto, Energy characterization of attitude algorithms, IEEE International Conference on Industrial Informatics, INDIN19 Proceedings (2019) 1585–1590.

[2] M.L. Hoang, A. Pietrosanto, A new technique on vibration optimization of industrial inclinometer for MEMS accelerometer without sensor fusion, IEEE Access 9 (2021) 20295–20304, http://dx.doi.org/10.1109/ACCESS.2021.3054825.

[3] G. Nutzi, S. Weiss, D. Scaramuzza, R. Siegwart, Fusion of IMU and vision for absolute scale estimation in monocular SLAM, J. Intell. Robot. Syst. 61 (2010) 287–299.

[4] M.L. Hoang, M. Carratù, M.A. Ugwiri, V. Paciello, A. Pietrosanto, A New technique for optimization of linear displacement measurement based on MEMS accelerometer, in: 2020 International Semiconductor Conference (CAS), Sinaia, Romania, 2020, pp. 155–158, http://dx.doi.org/10.1109/CAS50358.2020.9268038.

[5] S. Shin, D. Kim, Y. Seo, Controlling Mobile robot using IMU and EMG sensor-based gesture recognition, in: Ninth International Conference on Broadband and Wireless Computing, Communication and Applications, 2014.

[6] J.X. Cela Araguillin, K.E. Yánez Escarabay, M.F. Trujillo, A. Rosales, Mobile application for ergonomic analysis of the sitting posture of the torso, International Conference on Information Systems and Computer Science (2018).

[7] M. Kok, J.D. Hol, T.B. Schon, An optimization-based approach to human body motion capture using inertial sensors, in: Proceedings of the 19th World Congress of the International Federation of Automatic Control, Cape Town, South Africa, August, 2014, pp. 79–85.

[8] M.L. Hoang, A. Pietrosanto, An effective method on vibration immunity for inclinometer based on MEMS accelerometer, 2020 International Semiconductor Conference (CAS), Sinaia, Romania (2020) 105–108, http://dx.doi.org/10.1109/CAS50358.2020.9267997.

[9] B.J. Borbly, A. Tihanyi, P. Szolgay, A Measurement System For Wrist Movements In Biomedical Applications, 2015 European Conference on Circuit Theory and Design (ECCTD) (2015) 1–4.

[10] M.L. Hoang, A. Pietrosanto, A robust orientation system for inclinometer with full-redundancy in heavy industry, IEEE Sens. J. 21 (5) (2021) 5853–5860, http://dx.doi.org/10.1109/JSEN.2020.3040374, 1 March1.

[11] H. Debarba, L. Nedel, A. Maciel, LOP-cursor: fast and precise interaction with tiled displays using one hand and levels of precision, 2012 IEEE Symposium on 3D User Interfaces (3DUI) (2012) 125–132.

[12] T. Lisini Baldi, M. Mohammadi, S. Scheggi, D. Prat-tichizzo, U sing inertial and magnetic sensors for hand tracking and rendering in wearable haptics, 2015 IEEE World Haptics Conference (WHC) (2015) 381–387.

[13] P. Promrit, S. Chokchaitam, M. Ikura, In-vehicle MEMS IMU calibration using accelerometer, in: 2018 IEEE 5th International Conference on Smart Instrumentation, Measurement and Application (ICSIMA), Songkla, Thailand, 2018, pp. 1–3.

[14] Y. Zhong, Y. Xu, A calibration method of UAV accelerometer based on levenberg-marquardt iteration algorithm, in: 2018 Chinese Control And Decision Conference (CCDC), Shenyang, 2018, pp. 5634–5638.

[15] H. Ferdinando, H. Khoswanto, D. Purwanto, Embedded Kalman filter for Inertial Measurement Unit (IMU) on the ATMega8535, in: 2012 International Symposium on Innovations in Intelligent Systems and Applications, Trabzon, 2012, pp. 1–5.

[16] F. Abyarjoo, A. Barreto, J. Cofino, F.R. Ortega Implementing a Sensor Fusion Algorithm for 3D Orientation Detection with Inertial/Magnetic Sensors, Sobh T Elleithy K Innovations and Advances in Computing, Informatics, Systems Sciences, Networking and Engineering. Lecture Notes in Electrical Engineering, Vol. 313 Springer Cham.

[17] Z. Tan, Y. Wu, J. Zhang, Fused attitude estimation algorithm based on explicit complementary filter and Kalman filter for an indoor quadrotor UAV, in: 2018 Chinese Control And Decision Conference (CCDC), Shenyang, 2018, pp. 5813–5818.

[18] E.F. Helbling, S.B. Fuller, R.J. Wood, Pitch and yaw control of a robotic insect using an onboard magnetometer, in: 2014 IEEE International Conference on Robotics and Automation (ICRA), Hong Kong, 2014, pp. 5516–5522.

[19] Gang Shi, et al., An improved yaw estimation algorithm for land vehicles using MARG sensors, Sensors (Basel, Switzerland) 18 (10) (2018) 3251, 27 September.

[20] M. Carrat'u, S. Dello Iacono, A. Pietrosanto, V. Paciello, Imu selfalignment in suspensions control system, I2MTC 2019 - 2019 IEEE International Instrumentation and Measurement Technology Conference, Proceedings (2019) 861–866.

[21] M.S. Wahyudi, Listiyana, Sudjadi and Ngatelan, Tracking object based on GPS and IMU sensor, in: 2018 5th International Conference on Information Technology, Computer, and Electrical Engineering (ICITACEE), Semarang, 2018, pp. 214–218.

[22] Abha Damani, Hardik Shah, Krishna Shah, Global positioning system for object tracking, Int. J. Comput. Appl. (0975 – 8887) 109 (January (8)) (2015).

[23] E. Foxlin, Motion tracking requirements and technologies Handbook of Virtual Environment Technology, Vol. 8, 2002, pp. 163–210.

[24] S. Salah, E. M. Nebot, H. F. Durrant-Whyte, A high integrity IMU/GPS navigation loop for autonomous land vehicle applications Robotics and Automation IEEE Transactions on 15 572-578.

[25] S.A. Ludwig, Optimization of control parameter for filter algorithms for attitude and heading reference systems, in: 2018 IEEE Congress on Evolutionary Computation (CEC), Rio de Janeiro, 2018, pp. 1–8, http://dx.doi.org/10.1109/CEC.2018.8477725.

[26] M. Bulatowicz, et al., Laboratory search for a long-range T-Odd, P-Odd interaction from axionlike particles using dual-species nuclear magnetic resonance with polarized 129Xe and 131Xe gas, Phys. Rev. Lett. 111 (2013) 102001, September.

[27] H. Dong, Y. Gao, Comparison of compensation mechanism between an NMR gyroscope and an SERF gyroscope, IEEE Sens. J. 17 (13) (2017) 4052–4055, 1st July.

[28] N. O-larnnithipong, A. Barreto, Gyroscope Drift Correction Algorithm for Inertial Measurement Unit Used in Hand Motion Tracking, 2016, IEEE SENSORS, Orlando, FL, 2016, pp. 1–3.

[29] Y. Hsu, P. Chou, Y. Kuo, Drift modeling and compensation for MEMS-based gyroscope using a Wiener-type recurrent neural network, in: 2017 IEEE International Symposium on Inertial Sensors and Systems (INERTIAL), Kauai, HI, 2017, pp. 39–42.

[30] Yueyang Ben, Guisheng Yin, Wei Gao, F. Sun, Improved filter estimation method applied in zero velocity update for SINS, in: 2009 International Conference on Mechatronics and Automation, Changchun, 2009, pp. 3375–3380.

[31] S. Godha, G. Lachapelle, "Foot mounted inertial system for pedestrian navigation.", Meas. Sci. Technol. 19 (7) (2008), 075202.

[32] Antonio Ramón Jiménez, F. Seco, José Carlos Prieto, J. Guevara, Indoor pedestrian navigation using an INS/EKF framework for yaw drift reduction and a foot-mounted IMU., in: Positioning Navigation and Communication (WPNC), 2010 7th Workshop on, IEEE, 2010, pp. 135–143.

[33] S. Yong, C. Jiabin, S. Chunlei, H. Yongqiang, Research on the compensation in MEMS gyroscope random drift based on time-series analysis and Kalman filtering, in: 2015 34th Chinese Control Conference (CCC), Hangzhou, 2015, pp. 2078–2082.

[34] S.O.H. Madgwick, A.J.L. Harrison, R. Vaidyanathan, Estimation of IMU and MARG orientation using a gradient descent algorithm, IEEE International Conference on Rehabilitation Robotics (2011) 179–185.

[35] João Luís Marins, et al., An extended Kalman filter for quaternion-based orientation estimation using MARG sensors Intelligent Robots and Systems 2001, Proceedings. 2001 IEEE/RSJ International Conference on 4 (2001).

[36] S.A. Ludwig, K.D. Burnham, Comparison of euler estimate using extended kalman filter, madgwick and mahony on quadcopter flight data, in: 2018 International Conference on Unmanned Aircraft Systems (ICUAS), Dallas, TX, 2018, pp. 1236–1241.

[37] O. Sarbishei, On the accuracy improvement of low-power orientation filters using IMU and MARG sensor arrays, in: 2016 IEEE International Symposium on Circuits and Systems (ISCAS), Montreal, QC, 2016, pp. 1542–1545.

[38] M. Admiraal, S. Wilson, R. Vaidyanathan, Improved formulation of the IMU and MARG orientation gradient descent algorithm for motion tracking in human-machine interfaces, in: 2017 IEEE International Conference on Multisensor Fusion and Integration for Intelligent Systems (MFI), Daegu, 2017, pp. 403–410.

[39] H. Xing, Z. Chen, C. Wang, M. Guo, R. Zhang, Quaternion-based complementary filter for aiding in the self-alignment of the MEMS IMU, in: 2019 IEEE International Symposium on Inertial Sensors and Systems (INERTIAL), Naples, FL, USA, 2019, pp. 1–4.

[40] M. Selvarajan, C.M. Ananda, Quaternion based pointing algorithm for two-axis gimbal of micro aerial vehicles, in: 2016 IEEE International Conference on

Recent Trends in Electronics, Information & Communication Technology (RTEICT), Bangalore, 2016, pp. 1335–1339.
[41] T. Brunner, J. Lauffenburger, S. Changey, M. Basset, Quaternion-based IMU and stochastic error modeling for intelligent vehicles, in: 2015 IEEE Intelligent Vehicles Symposium (IV), Seoul, 2015, pp. 877–882.
[42] Y. Zhao, Cubature + extended hybrid kalman filtering method and its application in PPP/IMU tightly coupled navigation systems, IEEE Sens. J. 15 (December (12)) (2015) 6973–6985.
[43] S. Feng, G. Qiufen, G. Yuansheng, L. Junshan, Research on thermal characteristic in slow-small temperature changing for MEMS linear vibration gyroscope, in: 2006 International Conference on Mechatronics and Automation, Luoyang, Henan, 2006, pp. 475–479.
[44] STMicroelectronics, iNEMO Inertial Module: 3D Accelerometer, 3D Gyroscope, 3D Magnetometer - Data Sheet, March, 2015.
[45] STMicroelectronics, Ultra-low-power Arm® Cortex®-M4 32-bit MCU+FPU, 105 DMIPS, 512KB Flash/96KB RAM, 11 TIMs, 1 ADC, 11 comm. interfaces, January, 2015.
[46] STMicroelectronics, STM32F401xB/C And STM32F401xD/E Advanced Arm®-based 32-bit MCUs, December, 2018.
[47] STMicroelectronics, STM32 Nucleo-64 Boards - Product Specifications, October, 2018.
[48] STMicroelectronics, STM32 Nucleo-64 Boards - User Manual, December, 2017.
[49] STMicroelectronics, LSM9DS1 Adapter Board for a Standard DIL24 Socket, September, 2016.
[50] Rollins Road Burlingame, "Pan-Tilt Unit (Model PTU) User's Manual", Version 1.14, 10/24/2000.
[51] M.L. Hoang, A. Pietrosanto, S.D. Iacono, V. Paciello, Pre-processing technique for compass-less madgwick in heading estimation for industry 4.0, in: 2020 IEEE International Instrumentation and Measurement Technology Conference (I2MTC), Dubrovnik, Croatia, 2020, pp. 1–6, http://dx.doi.org/10.1109/I2MTC43012.2020.9128969.
[52] T. Chen, W. Hu, R. Sun, Displacement measurement algorithm using handheld device with accelerometer, in: 2010 Asia-Pacific Conference on Wearable Computing Systems, Shenzhen, 2010, pp. 122–126.

Biographies

Minh Long Hoang was born in Hanoi, Vietnam, in 1994. He received the B.S. degree in renewable energy from the University of Science and Technology of Hanoi, Vietnam in 2015 and the M.S. degree in electronic engineering in 2018 from University of Salerno, SA, Italy. Since Nov 2018, immediately after graduation from M.S. degree, he has been working on a Nationally Operative Program (PON) project of European Union about "Industry 4.0 oriented enhancement of Inertial Platform performance" as a PhD student at the University of Salerno, SA, Italy. Also within this project, he has been collaborating with Sensor System srl Company (Italy) and Baumer Company (Germany) as Researcher in R&D department in the field of inclinometer. His research interests include inertial measurement unit (IMU) sensors, microelectromechanical system (MEMS), real-time measurements, embedded systems and signal processing.

Antonio Pietrosanto (M'99-SM'12) was born in Naples, Italy, in 1961, has been full Professor of Electrical and Electronic Measurement at the University of Salerno, since 2001. He is been founder of three spin off of the University of Salerno: "SPRING OFF", "Metering Research" and "Hippocratica Imaging". His main research activities are in the fields of: Instrument Fault Detection and Isolation (IFDIA), sensors, WSNs, real-time measurements, embedded systems, metrological characterization of measurement software, advanced system for food quality inspection, image based measurements. He co-authored more than 150 papers international journals and conference proceedings.